29th Congress of the International Council of the Aeronautical Sciences
St. Petersburg, Russia; September 7-12, 2014

EFFICIENT JET NOISE PREDICTION USING SYNTHETIC EDDY METHOD AND BLOCK-STRUCTURED CARTESIAN MESH

Yuma Fukushima*
***Institute of Fluid Science, Tohoku University**

Abstract

In this study, an efficient jet noise prediction procedure is constructed. The proposed stochastic noise generation and radiation (SNGR) model consists of the Building-Cube Method solvers and a modified synthetic eddy method (SEM). The present method is applied to two test cases. The first case is the reconstruction of a wall-bounded turbulent field computed by direct numerical simulation (DNS). The second case is the noise prediction of subsonic round jet. The reconstructed spectrum of the wall-bounded flow agrees with the mean statistical data computed by DNS. The computational cost of the modified SEM is lower than existing turbulence generation methods. The prediction result of jet noise shows good agreement with experiment up to 6,000 Hz quantitatively. It is confirmed the proposed SNGR model achieves the high computational efficiency and also high prediction accuracy from the results of test cases.

1 Introduction

Broadband noise generated from the complicated jet flow is still main noise source of aircraft. By using large eddy simulation (LES) or direct numerical simulation (DNS) to compute near-field turbulent structures, an accurate noise prediction can be made [1]. However these approaches are too time consuming for industrial and design purposes. Therefore, computationally efficient and accurate methods of modeling turbulence are needed in order to study designs that reduce broadband noise of a jet flow. From this background, various methods to stochastically generate a turbulent velocity field have been proposed. These methods are computationally efficient and also provide time dependent turbulent fields which have prescribed flow features. These turbulence generation methods are practically employed in combination with Reynolds-averaged Navier-Stokes (RANS) and linearized Euler equations (LEE) simulations. This combined method is called stochastic noise generation and radiation (SNGR) model [2][3]. In this study, the SNGR model based on the block-structured Cartesian mesh method and synthetic eddy method (SEM) is constructed to realize the efficient jet noise prediction procedure.

RANS and LEE computations are conducted on the framework of block-structured Cartesian mesh method called Building-Cube Method (BCM) [4]. BCM has several advantages based on Cartesian mesh over body-fitted structured or unstructured mesh; quick mesh generation for complicated geometries, easy application of high order scheme, high efficiency in calculation and easy parallelization of process. BCM framework could accelerate the noise prediction processes.

SEM [5] is introduced to the procedure of stochastic turbulence generation to construct faster noise generation process. In the original SNGR model, the generation of a stochastic turbulent field is based on the superposition of random Fourier modes, assuming the von Karman-Pao energy spectrum. This assumption is not suitable for inhomogeneous flows such as a wall-bounded flow. On the other hand, SEM has the capability to suit any kind of flows. Moreover, a turbulence field is simply represented by the superposition of synthetic

eddies. Therefore, SEM is simple to implement and fast to compute like the random Fourier mode method.

The objective of this research is the construction of the efficient and accurate broadband noise prediction procedure. To achieve the computationally efficient process, the simulations of flow and sound fields are conducted on the BCM framework. Furthermore, the SEM is employed for the stochastic turbulence generation. The present method is applied to two test cases. The first case is the reconstruction of a wall-bounded turbulent field computed by DNS. The second case is the noise prediction of a subsonic round jet.

2 Numerical Method

2.1 Computational Mesh of BCM

Computational mesh of BCM is generated by following procedures [4]. Computational domain is divided into aggregation of square area named “Cube” as shown in Fig. 1(a). Each Cube is then divided by equi-spaced Cartesian mesh as shown in Fig. 1(b). Cells located outside the wall boundary are defined as fluid cells. On the other hand, cells located inside the wall boundary are defined as wall cells. In the method, all Cubes have the same number of cells so that the computational effort of all Cubes is basically equivalent in parallel computation and excellent parallel efficiency is achieved. Each Cube has three overlap cells as shown by hatched cells in Fig. 1(b) for data exchange. When mesh is locally refined, selected Cube for refinement is divided into eight Cubes, and each Cube is sub-divided by prescribed cells. After the refinement, the size of Cube is smoothed so that the size of adjacent Cubes is restricted to the same or double/half size.

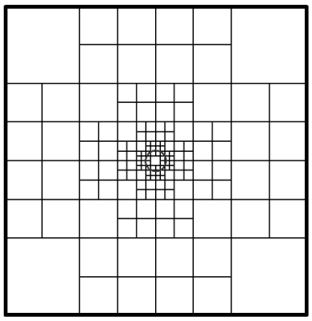

(a) Computational domain and Cube boundary

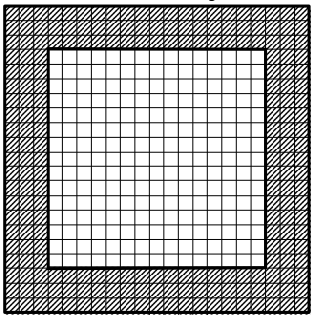

(b) Computational cells in a Cube (15×15 cells, 3 overlap cells)

Figure 1. Computational mesh of BCM in two-dimension

2.2 Stochastic Noise Generation and Radiation Model

The SNGR model is used as an aeroacoustic analysis method. The SNGR model can simulate the turbulent noise with lower computational cost in comparison with LES. Figure 2 shows the flowchart of the SNGR model. First, RANS simulation with a turbulence model provides a time-averaged flow field. Second, turbulent velocity fluctuations are generated by SEM using the flow information obtained from the RANS simulation. Third, LEE with unsteady source terms computed from turbulent velocity fluctuations is solved.

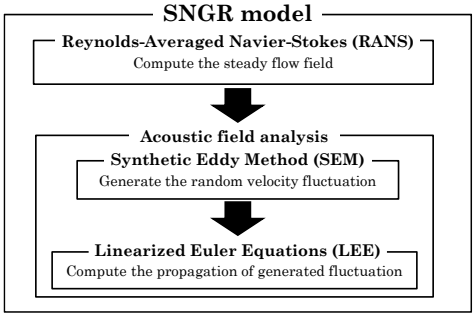

Figure 2. Flowchart of aeroacoustic analysis based on SNGR approach

2.3 Reynolds-Averaged Navier-Stokes Solver

The governing equations of computational fluid dynamics solver are the compressible Navier-Stokes equations, which are discretized using the cell-centered finite volume method. The simple low-dissipative AUSM (SLAU) [6] scheme is implemented to compute the inviscid flux. The spatial order is first order. For time integration, the lower-upper symmetric Gauss-Seidel (LU-SGS) implicit method is employed. Chien's standard k-ε turbulence model is used to close the equations [7]. Details of compressible BCM solver are described in Refs. [8] - [10].

2.4 Synthetic Eddy Method

The SEM is based on a superposition of a synthetic velocity signal which can be written as a sum of a finite number of eddies convecting with constant velocity (Fig. 3). This method is originally proposed to generate instantaneous velocity fluctuations at the inflow boundaries for LES or DNS applications. The advantages of SEM are easiness of implementation, lower computational cost in comparison with other methods, capability to suit any mesh and any kind of flows. The velocity fluctuations are generated by Eq. (1).

$$v_{i\,\mathrm{SEM}}^{n} = \frac{1}{\sqrt{N}} \sum_{k=1}^{N} A_{ij} \varepsilon_j^k f_{\sigma_{ij}}(\mathbf{x} - \mathbf{x}^k)$$

$$f_{\sigma_{ij}}(\mathbf{x}-\mathbf{x}^k) = \sqrt{V_B} \cdot \frac{1}{\sigma_{i1}} f\left(\frac{x_1 - x_1^k}{\sigma_{i1}}\right) \cdot \frac{1}{\sigma_{i2}} f\left(\frac{x_2 - x_2^k}{\sigma_{i2}}\right) \cdot \frac{1}{\sigma_{i3}} f\left(\frac{x_3 - x_3^k}{\sigma_{i3}}\right) \qquad (1)$$

$$A_{ij} = \begin{bmatrix} \sqrt{R_{11}} & 0 & 0 \\ R_{21}/A_{11} & \sqrt{R_{22} - A_{21}^2} & 0 \\ R_{31}/A_{11} & (R_{32} - A_{21}A_{31})/A_{22} & \sqrt{R_{33} - A_{31}^2 - A_{32}^2} \end{bmatrix}$$

where $\mathbf{x}$, $\mathbf{x}^k$ are the locations of mesh and the eddies. The ε_j^k are respective intensities of eddies and A_{ij} is the Cholesky decomposition of the prescribed Reynolds stress tensor. V_B is the volume of eddy box. σ is the turbulent length scale. The position of the eddies $\mathbf{x}^k$ before the first time step are independent from each other and taken from a uniform distribution over the box of eddies B and ε_j^k are independent random variables taken from any distribution with zero mean and unit variance. The shape function of synthetic eddy f is a linear tent function in this computation.

In the original SEM, each eddy convects with a constant velocity and time-dependency is introduced by the convection speed of eddies. However, this does not suit the SNGR model because the time scale is the same in all spatial directions. In the present method, independent turbulent velocity field is generated at each time step with Eq. (1) and a time-dependency is introduced by filtering using the Eq. (2) in each direction [11].

$$u_{i\,\mathrm{SEM}}^{n} = a_i u_{i\,\mathrm{SEM}}^{n-1} + b_i (v_{i\,\mathrm{SEM}}^{n} + v_{i\,\mathrm{SEM}}^{n-1})$$
$$a_i = \exp\left[1/(\tau_i \mathrm{F}_s)\right],\ b_i = \sqrt{(1 - a_i^2)/2} \qquad (2)$$

where F_s is the sampling frequency. The time scale $\tau_i = (\mathrm{f}_\tau)_i\, k/\varepsilon$ is calculated by the ratio of turbulent kinetic energy k to dissipation ratio ε. $(\mathrm{f}_\tau)_i$ is a turning parameter for adjusting the time scale response to prescribed computational or experimental data.

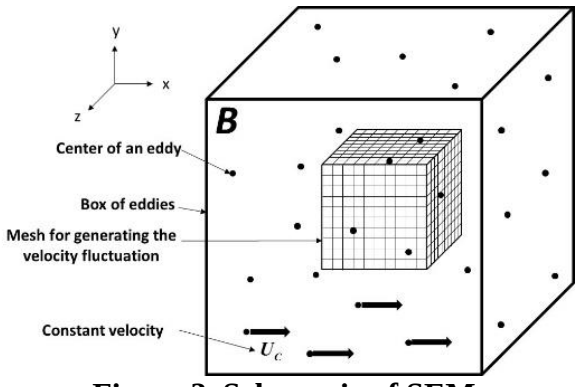

Figure 3. Schematic of SEM

2.5 Linearized Euler Equations Solver

Equations (3) and (4) represent the three-dimensional LEE. The LEE is a wave equation with advection and source terms, and thus is sufficient to compute the realistic sound propagation. In the computation of LEE, the mean flow field $\boldsymbol{Q_0}$ and sound source $\boldsymbol{S}$ are introduced as input data. Then, the time evolution of fluctuation component $\boldsymbol{Q'}$ is computed. The governing equations are nondimensionalized by the mean flow density, sonic speed and reference length.

$$\frac{\partial \boldsymbol{Q}'}{\partial t}+\frac{\partial \boldsymbol{E}}{\partial x_1}+\frac{\partial \boldsymbol{F}}{\partial x_2}+\frac{\partial \boldsymbol{G}}{\partial x_3}+\boldsymbol{H}=\boldsymbol{S}$$

$$\boldsymbol{Q}'=\begin{bmatrix}\rho'\\u'\\v'\\w'\\p'\end{bmatrix}\quad \boldsymbol{Q_0}=\begin{bmatrix}\rho_0\\u_0\\v_0\\w_0\\p_0\end{bmatrix}$$

$$\boldsymbol{E}=\begin{bmatrix}\rho_0u'+\rho'u_0\\u_0u'+\dfrac{p'}{\rho_0}\\u_0v'\\u_0w'\\u_0p'+\gamma p_0u'\end{bmatrix}\quad \boldsymbol{F}=\begin{bmatrix}\rho_0v'+\rho'v_0\\v_0u'\\v_0v'+\dfrac{p'}{\rho_0}\\v_0w'\\v_0p'+\gamma p_0v'\end{bmatrix}\quad \boldsymbol{G}=\begin{bmatrix}\rho_0w'+\rho'w_0\\w_0u'\\w_0v'\\w_0w'+\dfrac{p'}{\rho_0}\\w_0p'+\gamma p_0w'\end{bmatrix} \tag{3}$$

$$\boldsymbol{H}=\begin{bmatrix}0\\u'\left(\dfrac{\partial u_0}{\partial x_1}-\nabla\vec{v}_0\right)+\dfrac{1}{(\rho_0)^2}\left(\rho'\dfrac{\partial p_0}{\partial x_1}+p'\dfrac{\partial \rho_0}{\partial x_1}\right)\\v'\left(\dfrac{\partial v_0}{\partial x_2}-\nabla\vec{v}_0\right)+\dfrac{1}{(\rho_0)^2}\left(\rho'\dfrac{\partial p_0}{\partial x_2}+p'\dfrac{\partial \rho_0}{\partial x_2}\right)\\w'\left(\dfrac{\partial w_0}{\partial x_3}-\nabla\vec{v}_0\right)+\dfrac{1}{(\rho_0)^2}\left(\rho'\dfrac{\partial p_0}{\partial x_3}+p'\dfrac{\partial \rho_0}{\partial x_3}\right)\\(\gamma-1)\left[p'\nabla\vec{v}_0-\vec{v}'\nabla p_0\right]\end{bmatrix}$$

$$\boldsymbol{S}=\begin{bmatrix}0\\S_1-\overline{S_1}\\S_2-\overline{S_2}\\S_3-\overline{S_3}\\0\end{bmatrix} \tag{4}$$

$$S_i=-\frac{\partial \rho_0 u_{i\,\mathrm{SEM}}^n u_{j\,\mathrm{SEM}}^n}{\partial x_j},\ \overline{S_i}=-\overline{\frac{\partial \rho_0 u_{i\,\mathrm{SEM}}^n u_{j\,\mathrm{SEM}}^n}{\partial x_j}}$$

The spatial derivative is calculated by fourth-order dispersion relation preserving (DRP) scheme of seven-point stencils [12]. In addition, a fourth-order spatial filtering is applied in each iteration to eliminate the non-physical oscillations generated at the Cube boundary. Lagrange interpolation is employed for data exchange at the Cube boundary [13]. Time integration is performed by six-stage fourth-order low dissipation and dispersion Runge-Kutta (LDDRK) scheme [14]. The outgoing wave is damped by buffer zone boundary condition [15]. The sound source of Eq. (4) proposed by Bogey and Bailly is employed [16]. Details of BCM LEE solver are described in Refs. [17] - [19].

3 Reconstruction of Wall-Bounded Turbulent Field

The reconstruction of a wall-bounded turbulent field computed by DNS is conducted as the validation of the present stochastic turbulence generation method [20]. The mean statistical data of DNS is available from the European research community on flow, turbulence and combustion classic collection database [21]. The case of Reynolds number Re = 1,410 is chosen. Data consists of mean velocities and turbulent properties at a number of vertical locations. These are shown in Figs. 4 and 5. Energy spectra at y^+ = 100 are reported in the database. The turbulent field is generated by four methods, and the turbulent kinetic energy spectra of generated turbulent fields are compared with those of DNS result. In the random Fourier method, the turbulent field is generated by the superposition of the Fourier series [22]. The amplitude of each wave number is computed from the von Karman-Pao energy spectrum. In the digital filter method, the turbulent field is generated by the application of Gaussian filter to the white noise [23]. In the original SEM, turbulent field is generated by Eq. (1). In the modified SEM process, the nondimensional convection velocity is 16.329, R_{11} = 3.68, R_{22} = 1.19, R_{33} = 1.89 and R_{21} = -0.898 from Figs. 4 and 5. The resultant turning parameters are $(f_\tau)_1 = 4.0\times10^{-3}$, $(f_\tau)_2 = 0.9\times10^{-3}$ and $(f_\tau)_3 = 3.0\times10^{-3}$. To compare the computational time of each turbulence generation method, the turbulent field is generated 5,000 times on 10×10 meshes in all methods.

Figure 6 shows the computed turbulent kinetic energy spectra corresponding to the u velocity. Black line is the spectrum obtained from the DNS conducted by Spalart. The results of digital filter method and present method seem to agree the DNS data very well, with some discrepancies at the lower and higher wavenumber. On the other hand, the result of random Fourier overestimates in lower and higher wavenumbers. The result of original SEM has over- and underestimation in almost all wavenumbers. These results indicate that the present method has the capability to generate

the turbulent field based on the prescribed anisotropic Reynolds stress tensor and space-time correlation.

Table 1 shows the computational time to generate the turbulent field of Fig. 6. The digital filter method is most time consuming. On the other hand, the original SEM method has the lowest computational cost. The present method shows lower computational cost than the random Fourier method although Eq. (2) is added to the original SEM process. From these results, it is confirmed that modified SEM is suitable for the generation of velocity fluctuations in SNGR model.

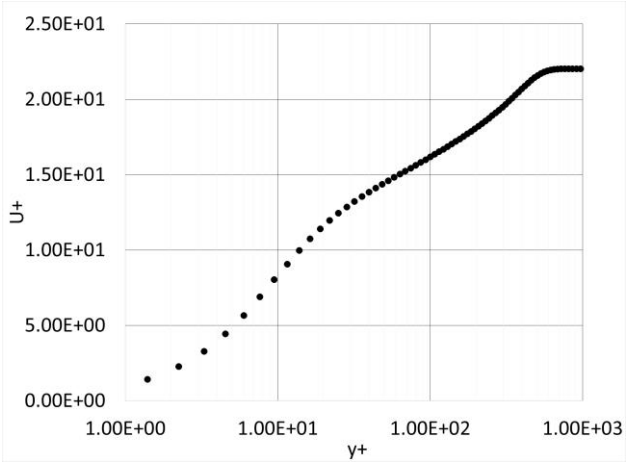

Figure 4. Mean velocity profile [17]

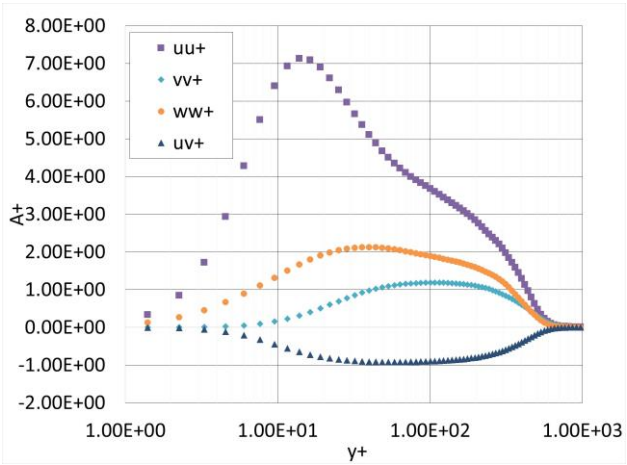

Figure 5. Reynolds stress profile [17]

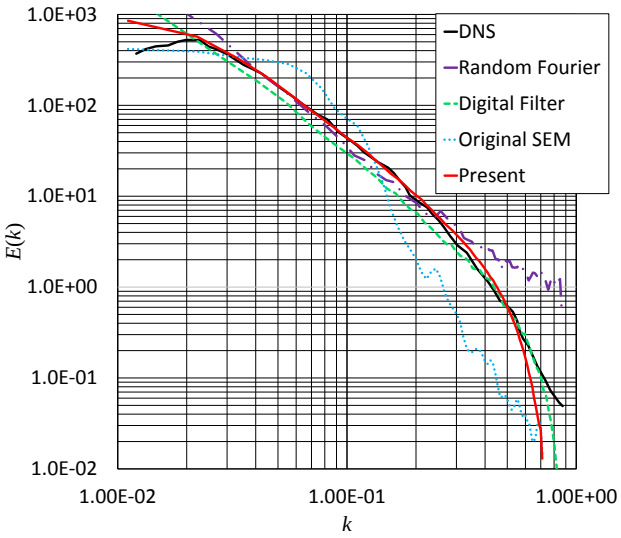

Figure 6. Turbulent kinetic energy spectra at y^+ = 100 corresponding to the *u* velocity

Table 1. Computational time

Method	Computational time [sec.]
Random Fourier	17.3
Digital Filter	224.1
Original SEM	8.0
Present	11.9

4 Noise Prediction of Subsonic Round Jet

The present SNGR model is applied to the noise prediction of a subsonic round jet [24][25]. The noise generated from a jet flow is computed and compared with experiment and with other's computational result. The jet Mach number M_{jet} = 0.72 and the diameter of the nozzle D = 80 mm. The computation is conducted with the background flow of M_∞ = 0.01 because flow into quiescent air is difficult to achieve the reasonable result. Reynolds number based on the diameter of the nozzle is Re = 5,601. Turbulent kinetic energy and the dissipation rate of RANS computation are used to generate the velocity fluctuation. The flow field is used as the background flow of LEE computation.

Velocity profile of a round jet, turbulent free-stream boundary condition of turbulence kinetic energy and dissipation ratio are computed by following equations [26].

$$
\begin{aligned}
&u_{in}(r) = M_{jet} \times \tanh\left[\frac{1}{a}\left(\frac{R}{r_{in}} - \frac{r_{in}}{R}\right)\right] \\
&a = 0.3 \\
&v_{in}(r) = w_{in}(r) = 0 \\
&k_{in} = 1.5 I^2 u_{in}^2 \\
&\varepsilon_{in} = C_\mu \frac{\rho k^2}{\mu}\left(\frac{\mu_t}{\mu}\right)^{-1} \\
&I = 0.01
\end{aligned}
\tag{5}
$$

where I is the turbulence intensity. r_{in} is the radius from jet centerline. R is jet radius. C_μ = 0.09 is the model coefficient of k-ε turbulence model. μ_t/μ is the eddy viscosity ratio. μ_t is the turbulent viscosity. μ is the molecular dynamic viscosity. μ_t/μ is set to 10 in this computation. Density and pressure are the same as far-field values. The computational region is one-quarter of jet domain due to flow symmetricity (Fig. 7). Computational domain is $400D \times 25D \times 25D$, number of Cubes are 386, total number of cells are 12.6 million and minimum cell size is $9.76 \times 10^{-2} D$.

Figures 8 and 9 show the u velocity and turbulent kinetic energy distribution of the cross-section surface. Jet flow spreads in a radial direction toward the downstream. Turbulent kinetic energy increases at the shear flow region.

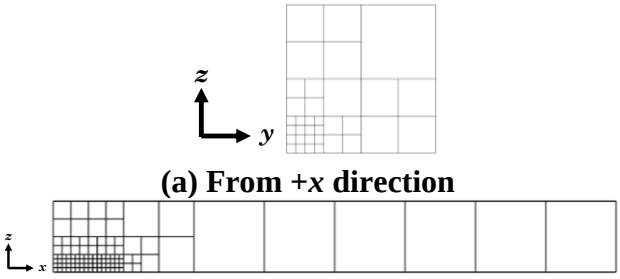

(a) From +x direction

(b) From –y direction

Figure 7. Computational domain of RANS computation

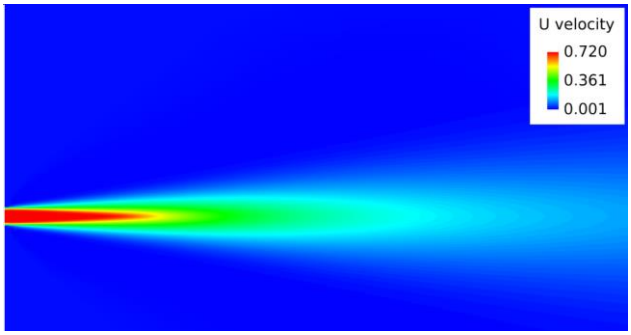

Figure 8. u velocity distribution

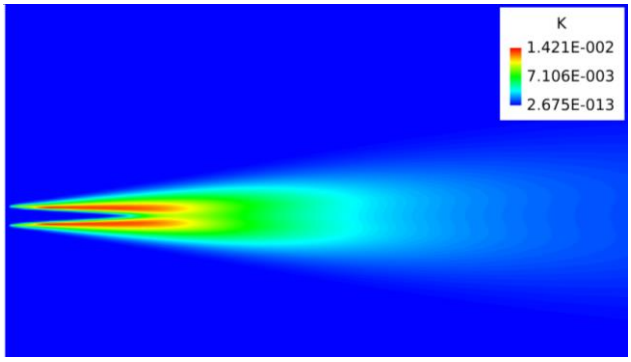

Figure 9. Turbulent kinetic energy distribution

The velocity fluctuation is generated by Eqs. (1) and (2) using the result of RANS computation. The number of eddies is N = 500 and the eddy shape f is modeled by linear tent function. The eddy box is set x = [-200D, -175D], y = [-3.125D, 3.125D], z = [-3.125D, 3.125D]. The nondimensional convection velocity is 0.72. The turbulent length scale is computed by following equation using local turbulent kinetic energy, the dissipation rate and cell size.

$$
\sigma_{i1} = \sigma_{i2} = \sigma_{i3} = \max\left(C_\mu \frac{k^{1.5}}{\varepsilon}, \Delta x\right) \tag{6}
$$

where Δx is the local cell size. Diagonal components of Reynolds stress tensor are computed by 2/3k and the other components are set zero. The turning parameter $(f_\tau)_i$ is set 1.0×10^{-3} in all directions.

The generated velocity fluctuation is used for the sound source represented in Eq. (4). The LEE computation is conducted without assuming flow symmetricity around jet axis. (Fig. 10) Computational domain is $400D \times 50D \times 50D$, the number of Cubes are 1,544, total number of cells are 50.6 million and

minimum cell size is $9.76\times10^{-2}D$. Figure 11 shows the pressure distribution generated from SEM procedure with turbulent kinetic energy contours of RANS computation. The sound source is the shear flow. The SEM successfully simulates the sound source of a jet flow. The generated noise propagates to far-field.

Figure 12 shows the definition of sampling points. Figure 13 shows the power spectral density (PSD) of the $r = 10D$ radius. The PSD at 45, 60, 70 and 80 deg are compared with experiment and Lafitte's computational results [25]. The computation of Lafitte is conducted based on SNGR model. However, the original turbulence generation method is employed [24]. Frequency is normalized by jet velocity V_{jet} = 244.8 m/s and reference length D = 0.08 m. PSD is also normalized by Strouhal number, St. St = 1 corresponds to 3,060 Hz.

The minimum cell size of LEE computation is 7.81×10^{-3} m. This cell size can resolve the sound wave up to 5,440 Hz using 10 cells. This frequency is the grid cut-off frequency of this computation. In Fig. 13, PSD is rapidly damped over this frequency. The minimum cell size of Lafitte's computation is 5.0×10^{-3} m and the grid cut-off frequency of this cell size is 8,500 Hz. The PSD of present method shows good agreement with experiment at all degree qualitatively. Highest PSD near St = 0.4 and negative slope near St = 1 are shown. However, the result at 45 deg is slightly overestimated compared with experiment and Lafitte's computational results. The sampling point of 45 deg is closest to sound source in the sampling points, and PSD is overestimated. This result can be improved by the modification of turbulent model because the standard k-ε turbulence model tends to estimate the peak of turbulent kinetic energy downstream compared with experiment in the jet flow computation [7]. The turbulent kinetic energy distribution changes according to the turbulent model.

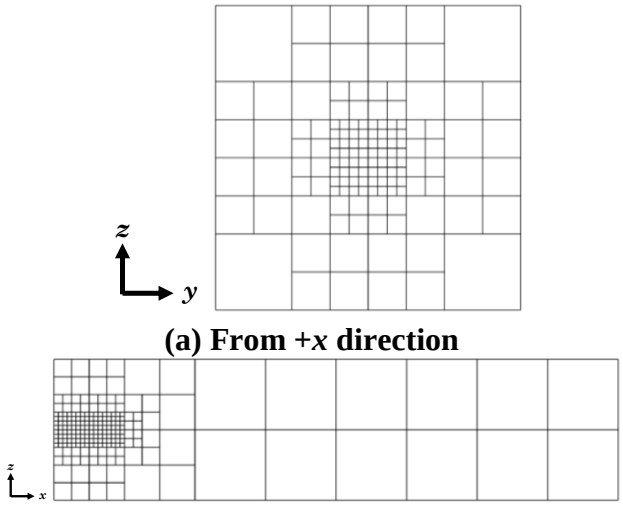

(a) From +x direction

(b) From –y direction

Figure 10. Computational domain of LEE computation

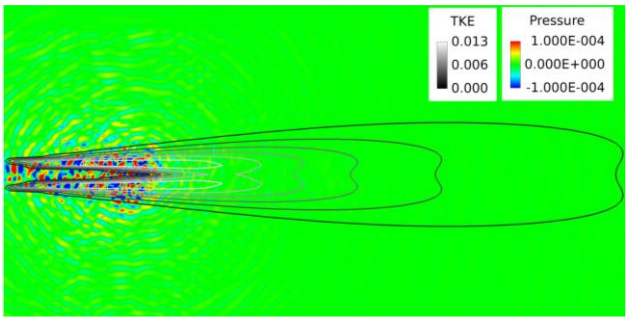

Figure 11. Pressure distribution with turbulent kinetic energy contours

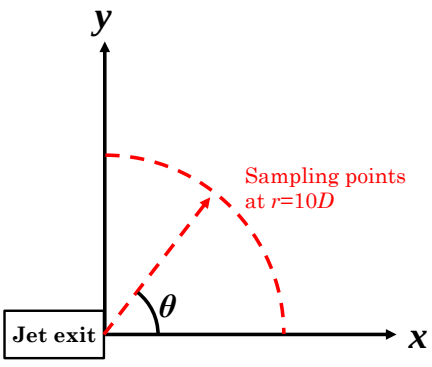

Figure 12. The definition of sampling points

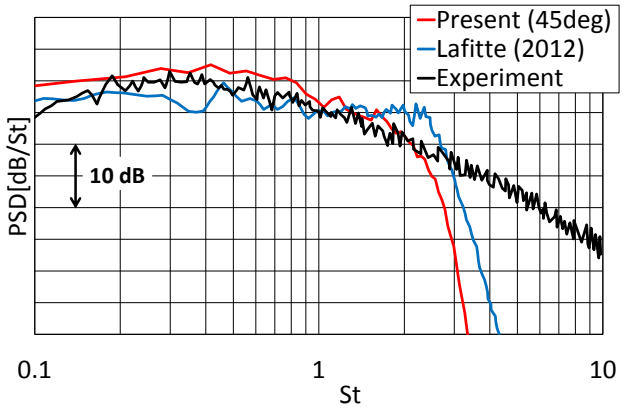

(a) 45deg

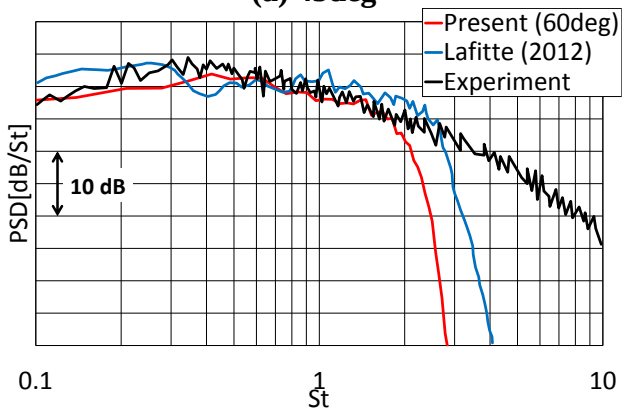

(b) 60deg

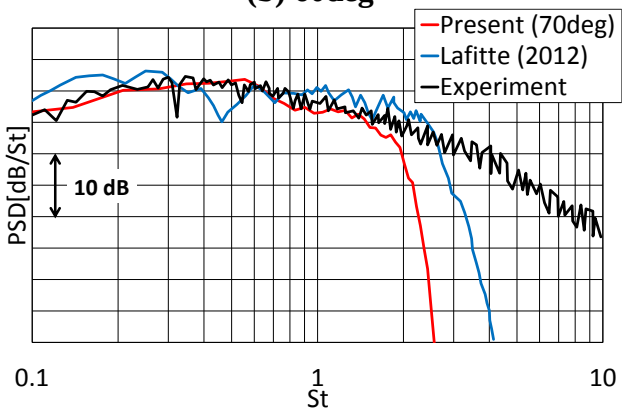

(c) 70deg

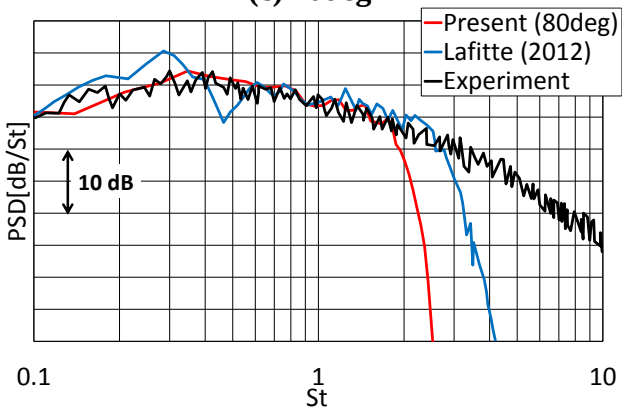

(d) 80deg

Figure 13. PSD distribution at $r = 10D$ radius

5 Conclusion

In this research, an efficient jet noise prediction procedure is constructed. The present SNGR model is employed to predict the turbulent noise generated from jet flow. RANS and LEE simulations are conducted on the BCM framework. The modified SEM is introduced to generate the velocity fluctuation.

The modified SEM is applied to the reconstruction of a wall-bounded turbulent field. Four turbulence generation procedures including the modified SEM are validated. The digital filter method and the modified SEM method provide better results compared with other turbulent generation methods. Moreover, the computational time of the modified SEM is much lower than the digital filter method. These results show the superiority of modified SEM.

The broadband noise generated from a round jet is predicted and compared with experimental and Lafitte's computational results. The predicted PSD shows good agreement with experiment at four angles of $r = 10D$ radius. Highest PSD near $St = 0.4$ and negative slope at $St = 1$ are shown. However, the result at 45 deg is slightly overestimated compared with experiment and Lafitte's computational result. This result can be improved by the modification of a turbulence model.

From the results of the test cases, it is confirmed the present SNGR model based on the BCM framework and the modified SEM is effective to jet noise prediction in terms of computational cost and prediction accuracy. RANS and LEE computations are based on the BCM framework and easily extended to large scale computation. The SEM realizes lower computational cost than existing methods, and can be implemented without sacrificing parallel efficiency of the LEE computation. The resultant SNGR model achieves the high computational efficiency and also high prediction accuracy.

References

[1] Paliath U., *et al.*, "Large Eddy Simulation for Jets from Chevron and Dual Flow Nozzles," 17th AIAA/CEAS Aeroacoustics Conference, AIAA Paper 2011-2881, Jun. 2011.

[2] Bailly, C., Juve, D., "A Stochastic Approach to Compute Subsonic Noise Using Linearized Euler's Equations," AIAA Paper 99-1872, 1999.

[3] Bechara, W., *et al.*, "Stochastic Approach to Noise Modeling for Free Turbulent Flows," *AIAA Journal*, Vol. 32, No. 3, pp. 455-463, 1994.

[4] Ishida, T., *et al.*, "Efficient and Robust Cartesian Mesh Generation for Building-Cube Method," *Journal of Computational Science and Technology*, Vol. 2, No. 4, pp. 435-446, 2008.

[5] Jarrin, N., *et al.*, "A Synthetic-Eddy-Method for Generating Inflow Conditions for Large-Eddy Simulations," *International Journal of Heat and Fluid Flow*, Vol. 27, No. 4, pp. 585-593, 2006.

[6] Shima, E., Kitamura, K., "On New Simple Low-Dissipation Scheme of AUSM-Family for All Speeds," 47th AIAA Aerospace Sciences Meeting, AIAA Paper 2009-136, Jan. 2009.

[7] Georgiadis, N. J., *et al.*, "Evaluation of Modified Two-Equation Turbulence Models for Jet Flow Predictions," 44th AIAA Aerospace Sciences Meeting, AIAA Paper 2006-490, Jan. 2006.

[8] Nakahashi, K., Kim, L., "High-Density Mesh Flow Computations by Building-Cube Method," *Computational Fluid Dynamics 2004*, pp. 121-126, 2006.

[9] Nakahashi, K., "Building-Cube Method for Flow Problems with Broadband Characteristic Length," *Computational Fluid Dynamics 2002*, pp. 77-81, 2003.

[10] Noshimoto, S., *et al.*, "RANS Simulation around Airfoils Using Building-Cube Method," 48th AIAA Aerospace Sciences Meeting, AIAA Paper 2010-710, Jan. 2010.

[11] Jones, R. F., *et al.*, "Stochastically generated Turbulence for Wall bounded Flows," ANZIAM Journal Vol. 51, pp. 541-554, 2010.

[12] Tam, C. K. W. "Recent advances in computational aeroacoustics," *Fluid Dynamics Research*, Vol. 38, No. 9, pp. 591-615, 2006.

[13] Ishida, T., *et al.*, "A High-Resolution Method for Flow Simulations on Block-Structured Cartesian Meshes," The Sixth International Conference on Computational Fluid Dynamics, 2010.

[14] Berland, J., *et al.*, "Low-dissipation and low-dispersion fourth-order Runge-Kutta algorithm," *Computers and Fluids*, Vol. 35, No. 10, pp. 1459-1463, 2006.

[15] Richards, S. K., *et al.*, "The Evaluation of Non-Reflecting Boundary Conditions for Duct Acoustic Computation," *Journal of Sound and Vibration*, Vol. 270, No. 3, pp. 539-557, 2004.

[16] Bogey, C., *et al.*, "Computation of Flow Noise Using Source Terms in Linearized Euler's Equations," AIAA Journal Vol. 40, No. 2, pp. 235-243, 2002.

[17] Fukushima Y., *et al.*, "Code Development of Linearized Euler Equation on Block-Structured Cartesian Mesh for Complicated Geometries," 50th AIAA Aerospace Sciences Meeting, AIAA Paper 2012-0832, Jan. 2012.

[18] Fukushima Y., *et al.*, "CFD-CAA Coupled Computation of Fan Noise Propagation from Engine Nacelle Based on Cartesian Mesh Method," 19th AIAA/CEAS Aeroacoustics Conference, AIAA Paper 2013-2020, May. 2013.

[19] Fukushima Y., *et al.* "The Numerical Analysis of Forward Fan Noise Shielding Effect on the Over-the-Wing Nacelle Configuration," 52nd Aerospace Sciences Meeting, AIAA Paper 2014-0720, Jan. 2014.

[20] http://cfd.mace.manchester.ac.uk/ercoftac/

[21] Spalart, P. R., "Direct Simulation of a Turbulent Boundary Layer up to Re(θ)=1,410," *Journal of Fluid Mechanics*, Vol. 187, No. 1, pp. 61-98, 1988.

[22] Lush, P., "Measurements of Subsonic Jet Noise and Comparison with Theory," *Journal of Fluid Mechanics*, Vol. 46, No. 3, pp. 477-500, 1971.

[23] Veloudis, I., *et al.*, "Novel implementation and Assessment of a Digital Filter Based Approach for the Generation of LES Inlet Conditions," Flow, Turbulence and Combustion, Vol. 74, No. 1, pp. 1-24, 2007.

[24] Lafitte, A., *et al.*, "A study based on the sweeping hypothesis to generate stochastic turbulence," 17th AIAA/CEAS Aeroacoustics Conference, AIAA Paper 2011-2888, Jun. 2011.

[25] Lafitte, A., *et al.*, "Prediction of subsonic jet noise relying on a sweeping based turbulence generation process," 18th AIAA/CEAS Aeroacoustics Conference, AIAA Paper 2012-2149, Jun. 2012.

[26] Faghani, E., *et al.*, "Numerical Investigation of Turbulent Free Jet Flows Issuing from Rectangular Nozzles: the Influence of small Aspect Ratio," Archive of Applied Mechanics, Vol. 80, No. 7, pp. 727-745, 2010.

Acknowledgements

The computation in this research was conducted by AltixUV2000 of Institute of Fluid Science, Tohoku University.

Copyright Statement